Journal of The Electrochemical Society, **161** (14) A1969-A1975 (2014)
0013-4651/2014/161(14)/A1969/7/$31.00 © The Electrochemical Society

Ternary Imidazolium-Pyrrolidinium-Based Ionic Liquid Electrolytes for Rechargeable Li-O_2 Batteries

Mahbuba Ara,[a] Tiejun Meng,[a,b] Gholam-Abbas Nazri,[b] Steven O. Salley,[a] and K. Y. Simon Ng[a,z]

[a]*Department of Chemical Engineering and Materials Science, Wayne State University, Detroit, Michigan 48202, USA*
[b]*Department of Physics and Astronomy, Wayne State University, Detroit, Michigan 48201, USA*

The conductivity and anodic stability of ternary mixed ionic liquid (IL) electrolytes consisting of pyrrolidinium [*N*-butyl-*N*-methylpyrrolidinium$^+$ (PYR_{14}^+)] and imidazolium [1-butyl-3-methylimidazolium$^+$ ($BMIM^+$)] based bis(trifluoromethylsulfonyl) imide ($TFSI^-$) with 0.5 M LiTFSI salt were investigated. PYR_{14}TFSI ionic liquid has been reported to be stable under an oxidative environment, while BMIMTFSI provides good ionic conductivity. A conductivity study of IL electrolytes revealed a linear correlation of conductivity as a function of IL – Li salt concentration and IL volume fraction. As a result, improved battery cycling in a mixture of 4:1 (80/20 v/v%) $BMIM^+$: PYR_{14}^+ was observed with a specific capacity of 330 mAh.g^{-1} over 50 cycles at a current density of 0.1 mA.cm^{-2}. Also, an EIS study revealed decreasing cathode polarization by demonstrating lower impedance values for ternary mixed electrolyte than that of the pure electrolytes upon cycling.

Manuscript submitted August 4, 2014; revised manuscript received September 2, 2014. Published September 23, 2014.

The commercial potential of Li-O_2 rechargeable batteries is tremendous due to their extremely high theoretical energy density of 12 kWh.kg^{-1} (excluding oxygen), which is comparable to that of gasoline.[1] For automotive applications, Li-O_2 battery technology may be viable if it can provide 1.7 kWh.kg^{-1} of energy to the wheels after losses from the battery chemistry. However, this technology is suffering with several issues related to electrodes and electrolyte such as lithium metal corrosion, electrolyte decomposition, wettability, cathode structure retention, catalyst selection, among others, which result in a large irreversibility and poor cycle life.[1,2] Previous reports on electrolytes[3–5] suggest that conventional carbonate based electrolyte decomposes during the discharge process to produce irreversible byproducts such as alkyl carbonates and lithium carboxylates; and during the charging process, the oxidative decomposition of these byproducts[6] lead to CO_2, CO, and other gases instead of O_2. It has been found that this decomposition process is favored by the highly reactive superoxide radical anion ($O_2^{\bullet-}$) formed through single-electron reduction of oxygen ($O_2 + e^- \rightarrow O_2^{\bullet-}$).[3,7,8] Ether-based electrolytes exhibit good stability for the first cycle but deteriorate upon cycling.[9–11] Another polar solvent, dimethyl sulfoxide (DMSO), is not stable against a Li anode as it can absorb moisture from the air.[12] Other recently studied electrolyte candidates are amides[13] and acetonitrile,[5] which are also not sufficiently stable against the oxygen radical to prevent autoxidation.[9,13]

As a potential electrochemically stable electrolyte for Li-O_2 batteries, ionic liquids (IL) are promising candidates due to their hydrophobicity, low volatility, low flammability, wide potential window, and high thermal stability. Among a variety of room temperature ionic liquid configurations, imidazolium[14–16] and pyrrolidinium[17–19] based ILs have attracted the most attention as next-generation Li-ion battery electrolytes. Pyrrolidinium salts of bis(trifluromethanesulfonul) imide (TFSI) have demonstrated high stability or low reactivity toward the superoxide radical anion.[20] Although PYR_{14}TFSI is stable, its high viscosity (100 centipoise) and low conductivity (1.4×10^{-3} S cm^{-1})[21] limit the diffusion rate of lithium ions in the electrolyte. On the other hand, various imidazolium based molten salts have demonstrated better cyclability compared to pyrrolidinium in lithium batteries[22] because of the higher ionic conductivity and lower viscosity.

Hence, a mixed imidazolium and pyrrolidinium based IL electrolyte could provide the stability and conductivity needed for both Li-air and high power Li-ion batteries (LIB). For instance, a ternary ionic liquid: 1-Ethyl-3-methylimidazolium bis(trifluoromethanesulfonyl) imide, N-cyanoethyl-N,N,N-trimethylammonium bis(trifluoromethanesulfonyl)imide, and LiTFSI, exhibited a discharge capacity close to the theoretical value with good compatibility with a $LiCoO_2$ cathode.[23] For Li-O_2 batteries, Cecchetto et al. investigated a mixture of PYR_{14}TFSI: TEGDME-$LiCF_3SO_3$ (1:1) and observed a lower overvoltage with higher conductivity for the electrolyte mixture than TEGDME alone.[24] However, the cyclability of this mixed electrolyte for Li-O_2 batteries was not reported. Up till now, there have been increasing efforts at developing new electrolytes; however, to the best of our knowledge, no ternary ILs based electrolyte for Li-O_2 batteries has been reported.

The present study aims to investigate ternary mixtures (IL_1-IL_2-Li-salt) of imidazolium and pyrrolidinium based ILs for Li-O_2 applications. BMIMTFSI was chosen as the imidazolium based IL as it has high ionic conductivity (4 mS.cm^{-1}) and lower viscosity (32 centipoise), whereas, PYR_{14}TFSI as a pyrrolidinium based IL as a stable solvent. Herein, different ternary mixtures of BMIMTFSI + PYR_{14}TFSI + 0.5 M LiTFSI were prepared to study the effect of IL composition on ionic conductivity, electrochemical stability, lithium transference number, and Li-O_2 battery performance. It was found that 4:1 (BMIMTFSI:PYR_{14}TFSI) mixed electrolyte enhanced both cyclic performance and columbic efficiency compared to BMIMTFSI or PYR_{14}TFSI used alone.

Experimental

Ternary mixtures of electrolyte preparation.— 1-butyl-3-methylimidazolium bis(trifluoromethylsulfonyl imide) (BMIMTFSI) (Sigma-Aldrich), and *N*-butyl-*N*-methylpyrrolidinium bis(trifluoromethanesulfonyl) imide (PYR_{14}TFSI) (TCI America) were used as room-temperature ionic liquids. The chemical structures are shown in Figure 1. These ionic liquids were dried in a vacuum at 323 K for more than 24 h and stored in a dry-argon-filled glove box ($[O_2] < 1$ ppm, $[H_2O] < 0.1$ ppm). Ionic liquid - lithium salt (lithium bis(trifluoromethanesulfonyl)-imide, LiTFSI, Sigma-Aldrich) binary mixture electrolytes were prepared by dissolving an appropriate amount of LiTFSI in ionic liquid. Ternary mixtures were prepared by mixing different ratios of BMIMTFSI and PYR_{14}TFSI ILs - 9:1 (90/10 v/v%), 4:2 (80/20 v/v%) and 7:3 (70/30 v/v%), and then dissolving an appropriate amount of LiTFSI Li-salt.

Conductivity measurement.— Conductivity of all pure and mixtures of ILs were determined using a digital conductivity meter (VWR International, LLC, model 2052). All tests were measured at room temperature inside the glove box.

Electrochemical stability measurement.— The electrochemical stability window of the LiTFSI-IL solutions was determined by linear sweep voltammetry (LSV) using a Gamry Reference 3000 Potentiostat

[z]E-mail: sng@wayne.edu

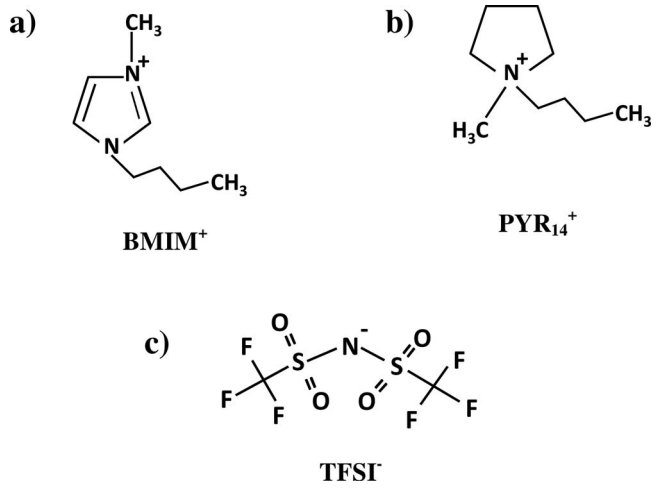

Figure 1. Schematic illustration of ions comprising the ILs (a) 1-butyl-3-methylimidazolium ($BMIM^+$), (b) *N*-butyl-*N*-methylpyrrolidinium (PYR_{14}^+) and (c) bis(trifluoromethanesulfonyl) imide ($TFSI^-$).

in two-electrode Teflon cells with Platinum as the working electrode (surface area 1.14 cm^2), lithium as the counter/reference electrode, and a Whatman (GF/D) glass fiber separator saturated with the IL electrolyte solution.

Li-O_2 battery electrode fabrication and cell configuration.—Carbon ink was prepared by mixing Ketjen Black (KB, ECD600JD, Akzo Nobel) carbon powders in DI water (H_2O)/isopropanol (IPA) solution with Nafion binder. 25 mg KB was physically mixed and added into 5 mL of an H_2O/IPA (3:1) solution with 0.1 mL Nafion dispersion (5 wt%, Ion Power, Inc.). Then the mixture was treated with ultrasonication for a minimum of 2 hours until it became a smooth ink in which no particles could be found. Circular disks of gas diffusion layer (F2GDL carbon paper, Fuel Cells Etc) with 0.5″ diameter (~0.255 mm thick) were put into the ink and sonicated for 15 minutes. Later, the carbon coated GDL was dried at 110°C in a vacuum oven for 12 h. The final carbon loading on the cathode was between 0.8 mg and 1 mg.

Li-O_2 cell assembly.— The Li-O_2 cell was comprised of a 7/16″ (diameter) circular lithium metal foil as the anode, a Whatman GF/D glass fiber separator, and the porous air cathode described above. A 0.5 M LiTFSI/IL (BMIMTFSI or, PYR_{14}TFSI or, the mixtures of ILs) electrolyte was used in the Li-O_2 cell. Lithium metal foils (99.9% pure, 0.75 mm thick, Alfa Aesar) were used as reference and counter electrode for the half-cell configuration. The cell construction was a spring loaded Swagelok design with active electrode areas of 1.15 cm^2, similar to the design by Beattie.[25] The cell was assembled in an argon-filled glove box with < 1 ppm oxygen and moisture content. Three cells of the same electrolyte were assembled for the cycling test and the average performance data were reported.

Characterization.— The crystalline product on the cathode structure after the first cycle (for discharge and charge, separately) was measured by X-ray diffraction (XRD) using a Rigaku SmartLab X-ray diffraction system. The morphology of the GDL (gas diffusion layer) surfaces after cycling was analyzed by field emission scanning electron microscopy (JEOL JSM-7600 FE-SEM). The cycled cells were disassembled in an Ar-filled glove box before measurements with XRD and FESEM. The cathodes were soaked in DMSO overnight and then dried under an Ar atmosphere.

Lithium ion transference number, T_{Li}^+, was determined by the method of ac impedance and dc polarization measurements using Li/electrolyte/Li cell,[26,27] where, Whatman GF/D glass fiber separator (530 micron thickness) was soaked with 100 μL electrolyte and then placed in a two-electrode cell between electrodes made of 7/16″ diameter of Lithium. According to this method, the lithium ion transference number could be calculated with the following equation:

$$T_{Li^+} = \frac{I_{ss}(\Delta V - I_0 R_0)}{I_{ss}(\Delta V - I_{ss} R_{ss})}$$

In this method, a small voltage, ΔV (<30 mV), is applied until a steady current (Iss) is obtained (time = 3000 s), I_0 is the initial current. R_0 and R_{ss} are the lithium interfacial resistance before and after polarization, respectively, measured by impedance spectroscopy in the 0.1–10^6 Hz frequency range.

Electrochemical cycling of the assembled cells was conducted galvanostatically using a Maccor battery tester (Maccor Inc., Model 4200) with a cutoff voltage range of 2.0 V–4.2 V while maintaining a constant current density. Electrochemical tests were performed under controlled atmospheric conditions using pure oxygen. The same cell was subjected to Electrochemical Impedance Spectroscopy (EIS) measurements (Gamry Instrument, Reference 3000) at the 0.1–10^6 Hz frequency range in order to measure the internal resistance build up during discharge-charge cycles.

Results and Discussion

Conductivity.— The ILs used for this study has different cations ($BMIM^+$ and PYR_{14}) and the same anion ($TFSI^-$) as shown in Figure 1. Figure 2a presents the ionic conductivity of Li salt in ionic liquid as a function of Li salt concentration. The ionic conductivity of BMIMTFSI decreased with increasing Li salt (LiTFSI) concentration. This is due to the increase of the viscosity of the IL-salt mixture with

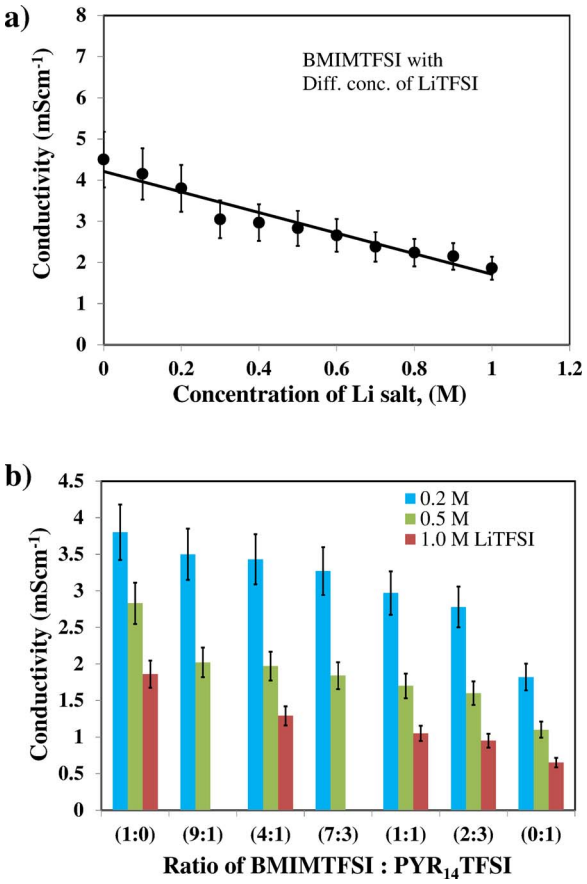

Figure 2. Conductivity of (a) BMIMTFSI IL with different Li salt (LiTFSI) concentration and (b) different ratio of ternary mixtures of BMIMTFSI and PYR_{14}TFSI ILs with 0.2 M, 0.5M, and 1M LiTFSI concentration.

Table I. Physical properties of different ternary mixture of BMIMTFSI:PYR_{14}TFSI ILs with 0.5 M LiTFSI.

$BMIM^+$: PYR_{14}^+ Ratio (v/v)	Ionic Conductivity ($mS.cm^{-1}$)	Anodic Stability (V)	Lithium Ion Transference Number (T_{Li}^+)
1:0	2.83	5.58	0.22
9:1	2.02	5.65	0.09
4:1	1.97	5.76	0.08
7:3	1.84	5.72	0.06
0:1	1.40	5.85	0.05

the increase in the concentration of LiTFSI, thus a resultant decrease in the mobility of ionic carriers in the electrolyte.[14]

Figure 2b shows the conductivities of different ratio of BMIMTFSI and PYR_{14}TFSI with 0.2, 0.5 and 1 M LiTFSI. Different ratios of the two cations ($BMIM^+$ and PYR_{14}^+) in the mixtures clearly indicate that the conductivity decreases with the increase of the fraction of PYR_{14}^+. This might be attributed to the increased viscosity with the increased fraction of PYR_{14}^+ in the mixtures. Previous reports found the conductivity of IL mixtures i.e., Li[NTf_2], [C_3C_1pyrr][NTf_2] and [C_3C_1pyrr][FSI] vary linearly with the $[FSI]^-$: $[NTf2]^-$ composition on a logarithmic scale with a fixed concentration of Li[NTf_2].[28] However, from all other studies, there is no fixed relationship has been established for the conductivity of ionic liquid mixtures.[29]

Lithium transference number.— The measured values of lithium transference number (T_{Li}^+) are presented in Table I. All electrolytes used were at 0.5 M LiTFSI concentration. As can be seen, T_{Li}^+ varies in the order of: BMIMTFSI (0.22) > 9:1 B: P (0.09) > 4:1 B: P (0.075) > 7:3 B: P (0.06) > PYR_{14}TFSI (0.05), following a similar trend with conductivity (Table I). Saito et al.[30] and Frömling et al.[31] calculated Li^+ transference numbers for BMIMTFSI and PYR_{14}TFSI as 0.1 and 0.06, respectively. It should be noted the molar ratios of IL/LiTFSI of 0.244 and 0.233 were used to calculate T_{Li}^+ from individual diffusion coefficients (calculated from NMR spectra) of cations and anions. Our findings suggest that T_{Li}^+ increases with the increase of $BMIM^+$ ions in the mixture. It has been found that in pyrrolidinium based IL, $TFSI^-$ anions are more strongly attracted to Li^+ cations than large PYR^+ cations and form ion clusters which increases the viscosity, leading to the reduced lithium ion diffusion and mobility in the electrolyte system.[31,32]

Electrochemical stability.— For lithium battery applications, it is very important to have a high electrochemical stability window (ESW) for the electrolytes. Linear sweep voltammetry (LSV) was conducted to investigate the electrochemical stability of the pure and mixtures of the IL electrolytes at room temperature. The anodic stability results are shown in Figure 3 for different ratio of BMIMTFSI and PYR_{14}TFSI ILs. The anodic stability of the electrolyte was measured from the open circuit voltage to positive voltage limit and the maximum stable potential was defined through the method of tangents.[33] In Figure 3, anodic (oxidation) stability voltages of the pure ILs of BMIMTFSI (B) and PYR_{14}TFSI (P) are 5.62 and 5.87 V vs. Li, while the mixtures have values of 5.65, 5.73 and 5.76 for 7:3, 9:1, and 4:1 of B:P, respectively. However, all of the ILs and their mixtures showed high anodic stability (compared to DMSO (4.8 V) and TEGDME (5.5 V))[34] which is very important for Li-O_2 cell applications, especially during charging. All of these electrolytes exhibit high oxidation stability against platinum electrode, whereas for other electrodes further study needs to be conducted.

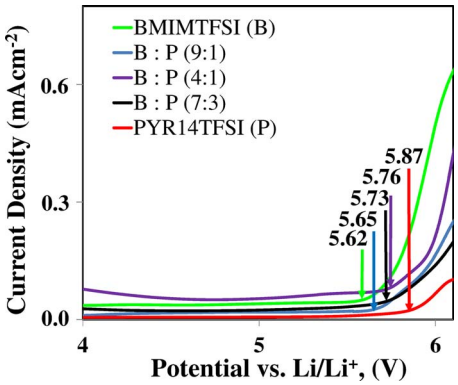

Figure 3. Anodic stability test of pure BMIMTFSI, PYR_{14}TFSI and different ternary mixtures of BMIMTFSI-PYR_{14}TFSI-LiTFSI (0.5 M) at a scan rate of 1 mV/s.

Electrochemical performance.— In order to delineate the correlation between the electrolyte compositions and the overpotentials of both ORR and OER, galvanostatic charge-discharge profiles on Li-O_2 batteries are presented. Figure 4a reports the first cycle discharge/charge curves of Li-O_2 cells with a KB carbon loaded GDL based cathode using two different binary mixtures of BMIMTFSI, PYR_{14}TFSI and three different ternary mixtures of 9:1, 4:1, and 7:3 $BMIM^+$: PYR_{14}^+ with 0.5 M LiTFSI, at a current density of 0.05 $mA.cm^{-2}$ (50 $mA.g^{-1}$ carbon). It can be seen that discharge occurs at almost the same voltage of 2.5 V (vs. Li^+/Li) for BMIMTFSI and 9:1, 4:1, and 7:3 $BMIM^+$: PYR_{14}^+ electrolytes and 2.4 V (vs. Li^+/Li) for PYR_{14}TFSI IL. Significant differences on charge voltages are apparent for the ternary IL electrolytes. Among all of the five electrolytes, 4:1 $BMIM^+$: PYR_{14}^+ shows the smallest overpotential value (0.3 V vs. Li^+/Li) and PYR_{14}TFSI has the largest (0.8 V vs. Li^+/Li) during the charge step. This is remarkably lower value of charge overpotential than that reported (0.44 and 0.6 V vs. Li^+/Li) previously in the literature.[21,24]

From Figure 4a, first cycle discharge capacities were found vary in the same manner as electrolyte conductivity (Table I): BMIMTFSI (7118 $mAh.g^{-1}$) > 9:1 (6829 $mAh.g^{-1}$) > 4:1 (4349 $mAh.g^{-1}$) > 7:3 (3064 $mAh.g^{-1}$) $BMIM^+$: PYR_{14}^+ > PYR_{14}TFSI (1468 $mAh.g^{-1}$). Similarly, pure $BMIM^+$, 9:1 and 4:1 $BMIM^+$: PYR_{14}^+ delivered higher first cycle charge capacities (more than 3200 $mAh.g^{-1}$) than 7:3 $BMIM^+$: PYR_{14}^+ (1496 $mAh.g^{-1}$) and pure PYR_{14}TFSI (1212 $mAh.g^{-1}$) electrolytes. These results clearly demonstrate that increasing PYR_{14}^+ in the electrolyte system significantly drops the specific capacity of the batteries. This can be attributed to the physicochemical properties of the electrolytes, i.e., ionic conductivity, viscosity, O_2 solubility, and wettability on the electrode. As indicated from the conductivity results, with 0.5 M LiTFSI in the mixture, PYR_{14}^+ based electrolyte become more viscous compared to $BMIM^+$, resulting in lower ionic conductivity (i.e., 1.1 $mS.cm^{-1}$ vs. 1.86 $mS.cm^{-1}$). As reported, oxygen diffusion coefficient is also lower for PYR_{14}TFSI (5.49×10^{-10} m^2 s^{-1}) than BMIMTFSI (8.76×10^{-10} m^2 s^{-1}).[35] This reduced mas transport of both Li^+ and O_2 limit the ORR reactions in the double-phase boundary in the cathode structure[6,36] and result in lower capacity.

Ternary mixture and pure ILs electrolyte cyclic performance.— Figures 4b, 4c, 4d, 4e and 4f illustrate the cyclability and charge/discharge profiles for neat ILs of BMIMTFSI, PYR_{14}TFSI and ternary mixtures of 9:1, 4:1, and 7:3 $BMIM^+$: PYR_{14}^+ tested at 0.1 $mA.cm^{-2}$ with 4 h of discharge time cutoff and charge from 2–4.2 V. For all of the cells, the depth of discharge was fixed at 400 $mAh.g^{-1}$ to limit the formation of discharge products and to maximize the cyclability. In the inset of Fig. 4b, it can be seen that neat BMIMTFSI shows a high charge capacity of 350 $mAh.g^{-1}$ with 87% coulombic efficiency in the first cycle and the cell demonstrated good cyclability until 17 cycles. The discharge plateau reduces after 20 cycles and charge capacity and efficiency gradually decrease, which suggests instability and decomposition of the electrolyte that creates reaction products other than Li_2O_2 and Li_2O.[2,7,8,36,37] After 25 cycles, the charge capacity decreased to 240 $mAh.g^{-1}$ with 60% coulombic efficiency.

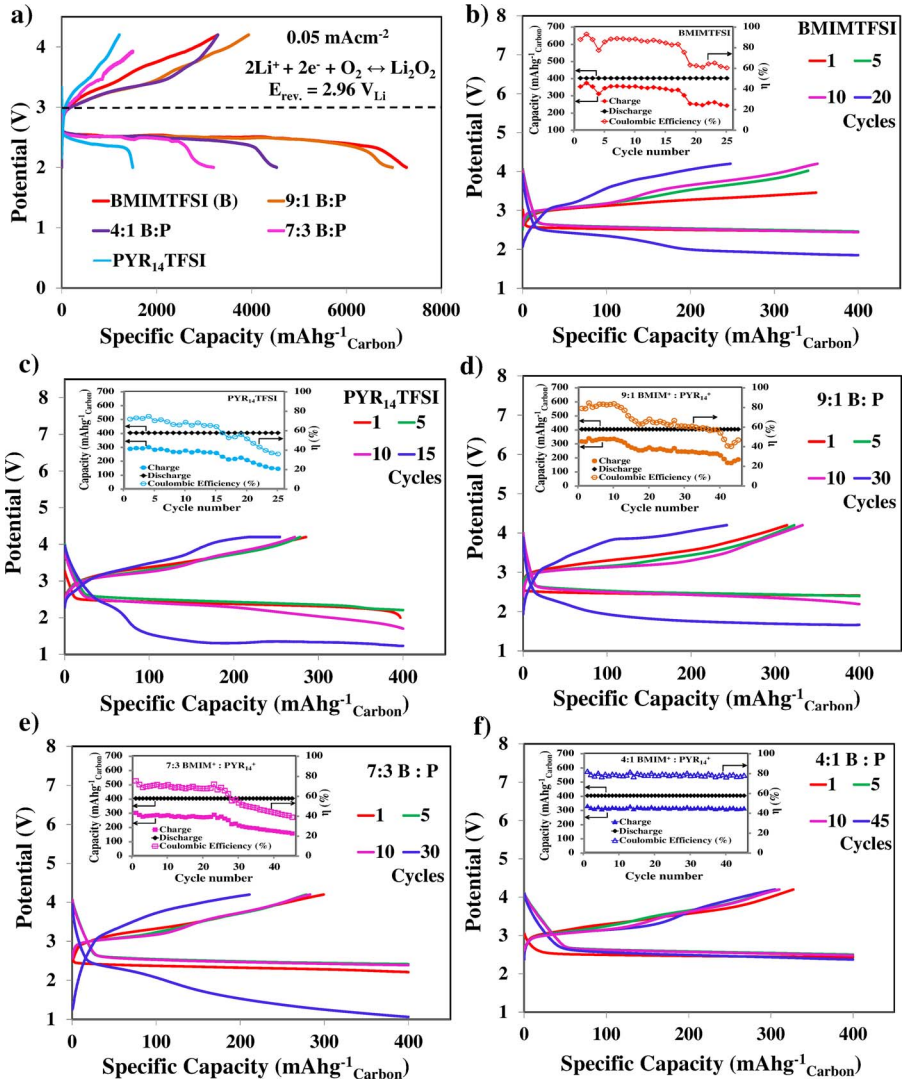

Figure 4. Initial discharge and charge profiles of different binary and ternary mixtures with 0.5 M LiTFSI at a current density of 0.05 mA/cm^2 (a), voltage profiles for different cycles at 0.1 mAcm^{-2} with 4 h discharge and charge voltage limit 4.2 V for (b) BMIMTFSI (B), (c) $PYR_{14}TFSI$ (P), (d) 9:1, (e) 7:3, and (f) 4:1, B:P, respectively. Inset pictures are charge and discharge capacity and coulombic efficiencies by cycle number of these five electrolytes.

Similar results can be observed from neat electrolyte cyclic performances of $PYR_{14}TFSI$ in Fig. 4c. For $PYR_{14}TFSI$ (inset Fig. 4c), the charge capacity (285 mAh.g^{-1}) is stable until 15 cycles with 71% coulombic efficiency which is higher than that reported (about 60% coulombic efficiency) previously.[21] However, the cell with $PYR_{14}TFSI$ shows a drastic reduction in discharge voltages below 2 V, resulting in a large overpotential which can be attributed to decreasing Li^+ ion mobility in the electrolytes upon cycling. Moreover, cycling may lead to an increase in electrolyte viscosity and poor O_2 diffusion. As a result, nonhomogeneous pore filling with the discharge products and thus clogging the porous cathode can occur.[38] The cell exhibits only 142 mAh.g^{-1} charge capacity with 35% coulombic efficiency after 25 cycles.

The effect of composition of ternary mixtures of $BMIM^+$ and PYR_{14}^+ based IL electrolytes on the cycling performances of Li-O_2 batteries is shown in Fig. 4d. As shown in the inset of Fig. 4d, the cell with 9:1 (90/10 v/v%) $BMIM^+$: PYR_{14}^+ electrolyte mixture gradually loses its capacity after the 10th cycle and shows only 73% (240 mAh.g^{-1}) of the initial charge capacity (327 mAh.g^{-1}). The discharge voltage (1.5 V) decreases drastically after the 30th cycle with an efficiency of 55%. The capacity fading and voltage instability can be attributed to imidazolium based ($BMIM^+$) electrolyte degradation with highly nucleophilic $O_2^{\bullet-}$ which results in the accumulation of the irreversible products on the Li-O_2 cathode.[39]

The cell with 7:3 (70/30 v/v%) $BMIM^+$: PYR_{14}^+ electrolyte mixture (Fig. 4e inset) retains 73% (220 mAh.g^{-1}) of the initial specific capacity (300 mAh.g^{-1}) after the 28th cycle. The coulombic efficiency also drops from 78 to 60%. The discharge voltage becomes much less than 2 V after the 28th cycle, which indicates large polarization of the electrode. These results indicate that the increase in the ratio of PYR_{14}^+ in the electrolyte mixture leads to higher viscosity and thus lowering the Li^+ ion conductivity.

Interestingly, the cell with 4:1 (80/20 v/v%) $BMIM^+$: PYR_{14}^+ ILs mixture (Fig. 4f inset) maintains a stable capacity up to 50 cycles which is 87% (285 mAh.g^{-1}) of the initial specific capacity (327 mAh.g^{-1}) and coulombic efficiency is maintained at 80%. This result suggests that an optimal mixture of BMIMTFSI and $PYR_{14}TFSI$ based ILs can simultaneously minimize decomposition while maintaining good ionic conductivity, thus enhance the cycling performance and coulombic efficiency. The capacity retention and cycling stability is much improved over that of previous ILs Li-O_2 studies (only about 200 mAh/g and stable for 15 cycles).[12,21] The discharge voltage remains stable at ~ 2.5 V and 45 cycles as shown in the inset Fig. 4f. The enhanced capacity retention is mainly due to improved Li^+ ion suppleness with lower viscosity (attributed to $BMIM^+$ in the electrolyte) which results in better O_2 diffusion in the porous cathode. From previous reports, pyrrolidinium based cation and $TFSI^-$/FSI^- based anions are proved to be stable with lithium/electrolyte/lithium system cyclability because of the formation of the solid-electrolyte interphase (SEI).[40,41] Therefore, the improved cyclability for the 4:1 $BMIM^+$:PYR_{14}^+ based cell may be attributed to the improved Lithium anode/electrolyte interface stability caused by the SEI passivation

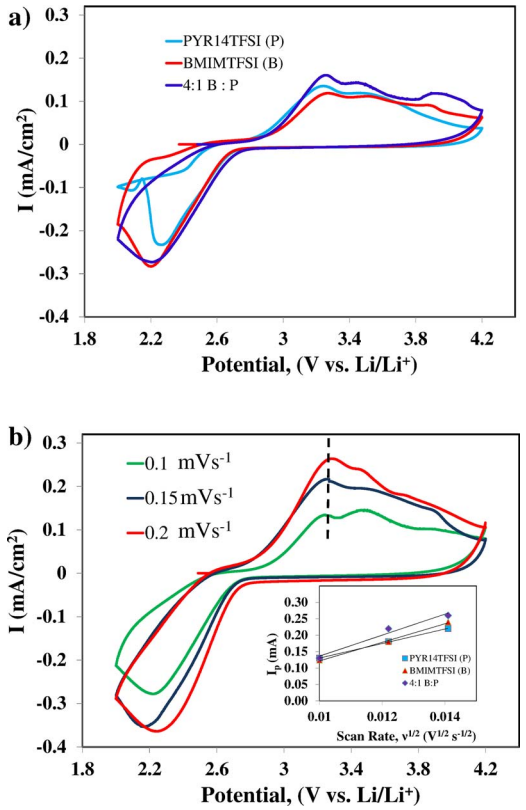

Figure 5. CV of Li-O_2 electrode using (a) BMIMTFSI (B), $PYR_{14}TFSI$ (P), and 4:1 B: P at 0.1 mVs^{-1} and (b) 4:1 B: P electrolyte at different scan rates, inset picture reports the peak current I_p versus the square root of the scan rate, $\nu^{1/2}$.

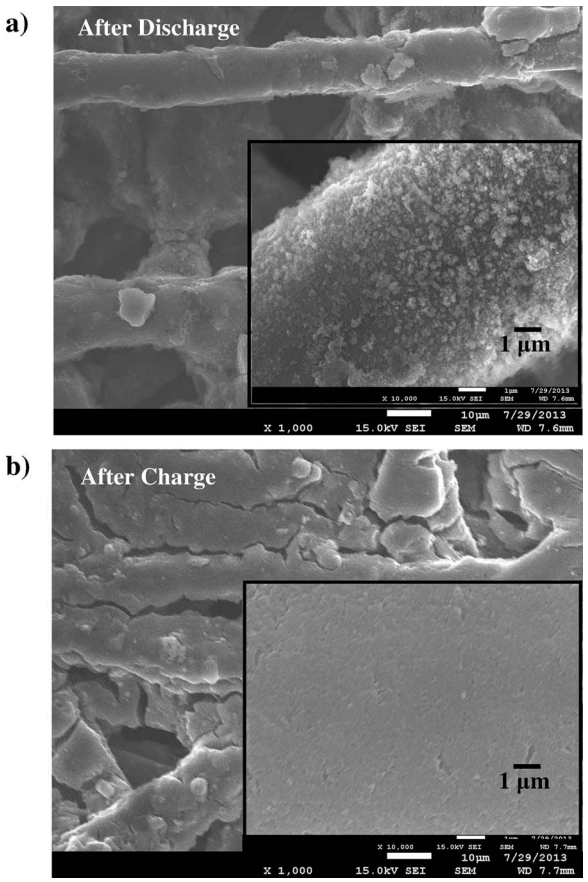

Figure 6. FE-SEM images of GDL after (a) first discharge and (b) first charge, respectively for Li-O_2 cell containing 4:1 ternary mixture of ionic liquid was fully discharged and charged at 0.1 $mAcm^{-2}$, voltage cutoff 2–4.2 V.

layer. Moreover, the superior voltage stability upon cycling is attributable to the reduction of parasitic reactions originating from the electrolyte decomposition with superoxide radicals.[20]

The enhanced reversibility of 4:1 $BMIM^+$: PYR_{14}^+ ternary mixture can be explained from cyclic voltammetry (CV) curves as shown in Figs. 5a and 5b. The anodic or cathodic peak voltages of 4:1 $BMIM^+$: PYR_{14}^+ mixture electrolytes agree with that obtained for BMIMTFSI and $PYR_{14}TFSI$ electrolytes. However, the oxidation/reduction peak current ratio for the mixture is higher than pure electrolytes, implying better reversibility.[42] CV curves display three different anodic peaks, indicating the formation of superoxide radicals along with the discharge products following the reactions: $O_2 + e^- \leftrightarrow O^{2\bullet-}$, $Li^+ + O_2 + e^- \leftrightarrow LiO_2$ and $O_2 + 2\ Li^+ + 2e^- \leftrightarrow Li_2O_2$. For the cell with 4:1 $BMIM^+$: PYR_{14}^+, the anodic and cathodic potentials remain unchanged with increased scan rate (Fig. 5b) which indicates that the reaction kinetics is not slow and reversible. Figure 5b (inset) displays the linear relationship between the anodic peak currents (I_p) and the potential scan rates ($\nu^{1/2}$) in the Randles-Sevicik plot which is also evident for diffusion controlled process. The Li^+ diffusion coefficient has been calculated as 3.06×10^{-8}, 1.86×10^{-8}, and 4.44×10^{-8} cm^2/s for BMIMTFSI, $PYR_{14}TFSI$, and 4:1 $BMIM^+$: PYR_{14}^+, respectively, using the Randles-Sevick equation: $I_p = [(269{,}000)\ n^{2/3} A D^{1/2} C]\ \nu^{1/2}$, where, n is number of electrons transferred in the redox event, A is electrode area, D is diffusion coefficient in cm^2/s, C is concentration of Li^+, ν scan rate in V/s. It is seen that diffusion coefficients in IL follows a Stokes-Einstein relationship[43] with viscosity (η), i.e. D α $1/\eta$. Hence, the high discharge capacity with good cycling performance is ascribed to the high diffusion coefficient (D) caused by the improvement of Li-ion diffusion for 4:1 BMIM: PYR_{14}^+.

In order to better comprehend the reaction products formed during the redox reactions at the Li-O_2 cathode with the 4:1 $BMIM^+$: PYR_{14}^+ electrolytes, XRD and FESEM analysis were performed. From the FESEM images of the GDL air-cathode (Fig. 6), it can be observed that some white crystals are formed on the carbon surface after first discharge, which, from the XRD results, is mostly Li_2O_2. After first charge, the carbon displays a very smooth surface without the evidence of any crystals, indicating complete reversibility.

From the XRD patterns (Fig. 7), after first discharge (b), it can be concluded that the dominant discharge (ORR) product is Li_2O_2. Two low intensity peaks of Li_2CO_3 are detected as well. Li_2CO_3

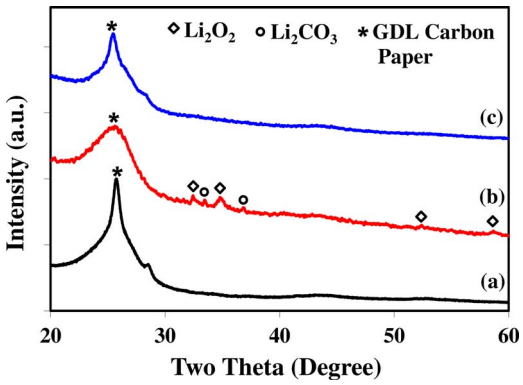

Figure 7. XRD pattern of air-electrode performed before cycling (a), after discharge (b) and charge (c), respectively. Li-O_2 cell containing 4:1 ternary mixture of ionic liquid was fully discharged and charged at 0.1 $mA \bullet cm^{-2}$ with voltage cutoff 2–4.2 V.

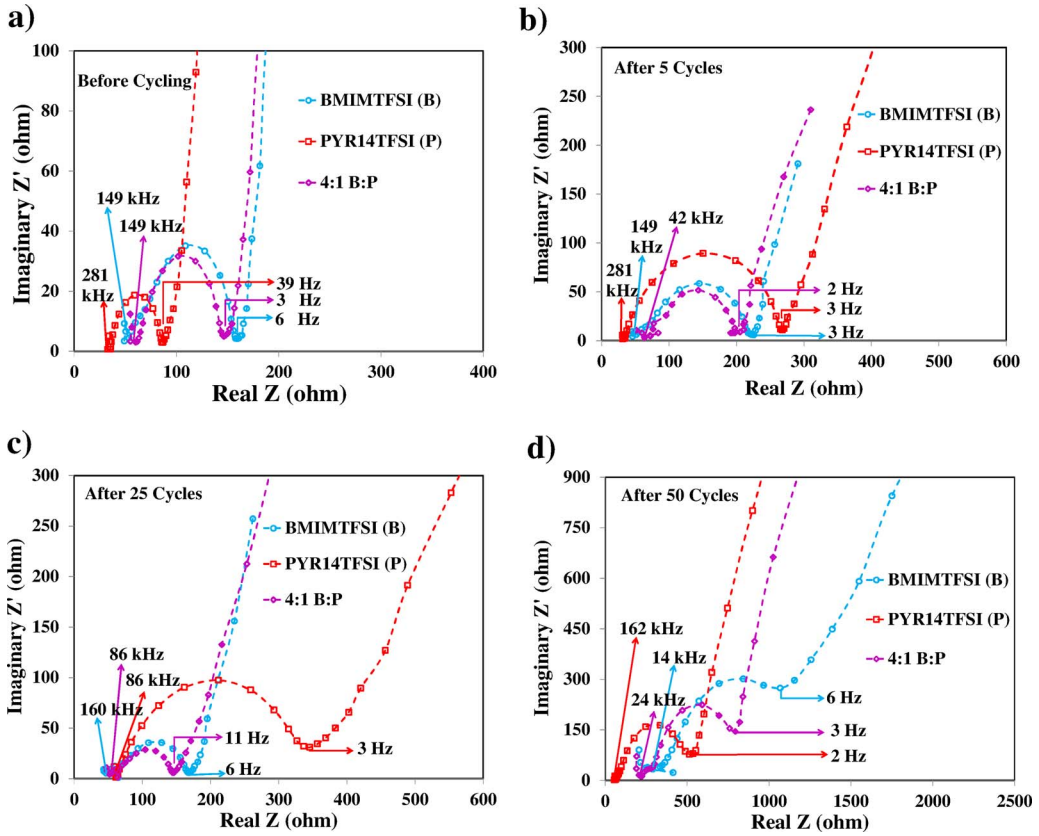

Figure 8. Nyquist plots of BMIMTFSI (B), $PYR_{14}TFSI$ (P), and ternary mixture of 4:1 B: P with 0.5 M LiTFSI cycled at 0.1 $mAcm^{-2}$ with 4 h discharge and charge voltage limit 4.2 V at (a) before cycling, after (b) 5, (c) 25 and (d) 50 cycles.

can originate from the initially formed Li_2O_2: $Li_2O_2 + C + \frac{1}{2} O_2 => Li_2CO_3$ or, $2Li_2O_2 + C => Li_2O + Li_2CO_3$. However, after first charge (Fig. 7c) no detectable peaks are identified, suggesting that both Li_2O_2 and Li_2CO_3 reversibly oxidized during the charge cycle. This result indicates a complete reversible charge/discharge cycle without electrolyte degradation during reduction.

Electrochemical impedance spectroscopy.— To further examine the cathode/electrolyte interface behavior, the electrochemical impedance spectroscopy of Li-O_2 cells was measured at different discharge/charge cycles. Typical Nyquist plots for impedance are shown in Figs. 8a–8d. It is seen that all semicircles in the Fig. 8 are not depressed and appears to consist of only one semicircle. The impedance spectra fit the equivalent circuit shown in Fig. 8a inset. Ohmic resistance (R_S) values correspond to the intercepts with the real axis at the highest frequencies and can be attributed to the electrolyte, electrode/collector contacts, and electrodes. The charge transfer resistance (R_{ct}) and constant phase element (CPE) corresponds to the resistance due to oxygen reduction reaction and double-layer capacitance, respectively. Warburg impedance (W) is attributed to the ionic diffusion process. All the values of R_{ct} for three electrolytes before and after multiple cycles are presented in Table II. Before cycling (Fig. 8a), $PYR_{14}TFSI$ shows lower resistance values for both R_S and R_{ct} than that of BMIMTFSI and 4:1 $BMIM^+$: PYR_{14}^+ ternary electrolyte, which might be attributed to the better wettability of the former electrolyte of the cathodes.[44]

After 5 cycles (Fig. 8b), the R_{ct} increases among all of the four electrolytes in the order of $PYR_{14}TFSI$ (239 Ω) > BMIMTFSI (171 Ω) > 4:1 $BMIM^+$: PYR_{14}^+ (139 Ω) and R_s values remain unchanged for all electrolytes. After 25 cycles (Fig. 8c), the R_{ct} increases following the same order of 5 cycling: $PYR_{14}TFSI$ (281 Ω) > BMIMTFSI (208 Ω) > 4:1 $BMIM^+$: PYR_{14}^+ (110 Ω). On the other hand, R_s remains unchanged for BMIMTFSI and 4:1 $BMIM^+$: PYR_{14}^+ and increases for $PYR_{14}TFSI$. The augmentation of R_{ct} after cycling might be ascribed to the clogging of the pores from the decomposition of the electrolyte and deposition of the discharge products, resulting in sluggish oxygen reduction reaction kinetics and diffusion of Li^+ and O_2 to the electrode surface.[24,45] Impedance associated with the passivation of the cathode surface by the electronically insulating discharge products can also be responsible for the increased Rct values after cycling.[46] In the case of 4:1 $BMIM^+$: PYR_{14}^+ ternary electrolyte, both Rs and Rct were lower after 25 cycles than after 5 cycles. This finding suggests that the optimum ratio of PYR_{14}^+ with $BMIM^+$ can minimize the electrode/electrolyte interface interactions and thus improve the rechargeability of Li-O_2 batteries.

After 50 cycles (Fig. 8d), impedance (R_{ct}) increases considerably for all of the cells with three electrolytes: BMIMTFSI (769 Ω) > 4:1 $BMIM^+$: PYR_{14}^+ (556 Ω) > $PYR_{14}TFSI$ (472 Ω). This large increase in the impedance for all electrolytes indicates oxygen electrode polarization and electrolyte decomposition. $PYR_{14}TFSI$ and 4:1 $BMIM^+$: PYR_{14}^+ exhibit lower values of R_{ct} than BMIMTFSI, which might be attributed to the higher degree of electrolyte degradation for imidazolium based IL than pyrrolidinium after prolonged cycling.

Table II. AC impedance spectroscopy results of the charge-transfer resistance (R_{ct}) values of Li-O_2 cells in BMIMTFSI (B), $PYR_{14}TFSI$ (P), and 4:1 B: P electrolytes at different cycles.

	R_{ct} (Ω)			
Electrolytes	Before Cycling	After 5 Cycles	After 25 Cycles	After 50 Cycles
BMIMTFSI (B)	105	171	208	769
$PYR_{14}TFSI$ (P)	53	239	281	472
4:1 B:P	89	139	110	556

Conclusions

Physical and electrochemical properties of pure and ternary mixtures of pyrrolidinium and imidazolium based ILs were investigated. Conductivity and lithium transference number of the ternary mixtures demonstrate higher values and fair anodic stability compared to pure $PYR_{14}TFSI$ IL. 4:1 $BMIM^+$: $PYR_{14}{}^+$ IL represents the highest rechargeability and efficiency of the Li-O_2 cell with the largest capacity retention among all electrolytes mixtures. The reversibility of this optimal electrolyte is also evident from the CV, FESEM and XRD patterns, where Li_2O_2 and Li_2CO_3 are identified in the discharged cell, which are reoxidized during the first charge cycle. The EIS study also revealed reduced electrode polarization for the optimum ratio (4:1 $BMIM^+$: $PYR_{14}{}^+$) of ILs in the mixture after 25 cycles. The rechargeability of the Li-O_2 cell has been demonstrated for 50 cycles with high coulombic efficiency in this study, which can be attributed to the synergistic effects of enhanced stability and conductivity from the 4:1 $BMIM^+$:$PYR_{14}{}^-$ IL.

Acknowledgment

Financial support from the Department of Energy (Grant DE-EE0002106) for this research is gratefully acknowledged.

References

1. M. Armand and J. M. Taracson, *Nature*, **451**, 652 (2008).
2. T. Ogasawara, A Pebart, M. Holzapfel, P. Novak, and P. G. Bruce, *J. Am. Chem. Soc.*, **128**, 1390 (2006).
3. S. A. Freunberger, Y. Chen, Z. Peng, J. M. Griffin, L. J. Hardwick, F. Barde, P. Novak, and P. G. Bruce, *J. Am. Chem.Soc.*, **133**, 8040 (2011).
4. W. Xu, V. V. Viswanathan, D. Wang, S. A. Towne, J. Xiao, Z. Nie, D. Hu, and J. G. Zhang, *J. Power Sources*, **196**, 3894 (2011).
5. C. O. Laoire, S. Mukerjee, K. M. Abraham, E. J. Plichta, and M. A. Hendrickson, *J. Phys. Chem. C*, **114**, 9178 (2010).
6. D. Capsoni, M. Bini, S. Ferrari, E. Quartarone, and P Mustarelli, *J. Power Sources*, **220**, 253 (2012).
7. B. D. McCloskey, D.S. Bethune, R.M. Shelby, G. Girishkumar, and A.C. Luntz, *J. Phys. Chem. Lett.*, **2**, 1161 (2011).
8. R. Black, S.H. Oh, J. Lee, T. Yim, B. Adams, and L.F. Nazar, *J. Am. Chem. Soc.*, **134**, 2902 (2012).
9. S. A. Freunberger, Y. Chen, N. E. Drewett, L. J. Hardwick, F. Bardé, and P. G. Bruce, *Angew. Chem., Int. Ed.*, **50**, 8609 (2011).
10. B. D. McCloskey, A. Speidel, R. Scheffler, D. C. Miller,V. Viswanathan, J. S. Hummelshoj, J. K. Nørskov, and A. C. Luntz, *J. Phys. Chem. Lett.*, **3**, 997 (2012).
11. B. M. Gallant, R. R. Mitchell, D. G. Kwabi, J. Zhou, L. Zuin, C. V. Thompson, and Y. Shao-Horn, *J. Phys. Chem. C*, **116**, 20800 (2012).
12. Z. Peng, S. A. Freunberger, Y. H. Chen, and P. G. Bruce, *Science*, **337**, 563 (2012).
13. Y. Chen, S. A. Freunberger, Z. Peng, F. Barde, and P. Bruce, *J. Am. Chem. Soc.*, **134**, 7952 (2012).
14. S. Seki, Y. Ohno, Y. Kobayashi, H. Miyashiro, A. Usami, Y. Mita, H. Tokuda, M. Watanabe, K. Hayamizu, S. Tsuzuki, M. Hattori, and N. Terada, *J. Electrochem Soc.*, **154**, A173 (2007).
15. H. Srour, H. Rouault, and C. Santini, *J. Electrochem Soc.*, **160**, A66 (2013).
16. J. Kim, A. Matic, J. Ahn, and P. Jacobsson, *J. Power Sources*, **195**, 7639 (2010).
17. G. B. Appetecchi, M. Montanino, D. Zane, M. Carewska, F. Alessandrini, and S. Passerini, *Electrochim. Acta*, **54**, 1325 (2009).
18. C. Arbizzani, G. Gabrielli, and M. Mastragostino, *J. Power Sources*, **196**, 4801 (2011).
19. S. Tan, Y. J. Ji, Z. R. Zhang, and Y. Yang, *ChemPhysChem*, **15**, 1956 (2014).
20. J. Herranz, A. Garsuch, and H. A. Gasteiger, *J. Phys. Chem. C*, **116**, 19084 (2012).
21. F. Soavi, S. Monaco, and M. Mastragostino, *J. Power Sources*, **224**, 115 (2013).
22. A. Lewandowski and A. Świderska-Mocek, *J. Power Sources*, **194**, 601 (2009).
23. M. Egashira, M. Tanaka-Nakagawa, I. Watanabe, S. Okada, and J. I. Yamaki , *J. Power Sources*, **160**, 1387 (2006).
24. L. Cecchetto, M. Salomon, B. Scrosati, and F. Croce, *J. Power Sources*, **213**, 233 (2012).
25. S. D. Beattie, D. M. Manolescu, and S. L. Blair, *J. Electrochem. Soc.*, **156**, A44 (2009).
26. J. Evans, C. A. Vincent, and P. G. Bruce, *Polymer*, **28**, 2324 (1987).
27. P. G. Bruce and C. A. Vincent, *J. Electroanal. Chem.*, **225**, 1 (1987).
28. P. M. Bayley, A. S. Best, D. R. MacFarlane, and M. Forsyth, *ChemPhysChem*, **12**, 823 (2011).
29. H. Niedermeyer, J. P. Hallett, I. J. Villar-Garcia, P. A. Hunt, and T. Welton, *Chem. Soc. Rev*, **41**, 7780 (2012).
30. Y. Saito, T. Umecky, J. Niwa, T. Sakai, and S. Maeda, *J. Phys. Chem. B*, **111**, 11794 (2007).
31. T. Frömling, M. Kunze, M. Schönhoff, J. Sundermeyer, and B. Roling, *J. Phys. Chem. B*, **112**, 12985 (2008).
32. R. Kühnel and A. Balducci, *J. Phys. Chem. C*, **118**, 5742 (2014).
33. C. Liew and S. Ramesh, *Materials*, **7**, 4019 (2014).
34. D. Xu, Z. Wang, J. Xu, L. Zhang, L. Wang, and X. Zhang, *Chem. Commun.*, **48**, 11674 (2012).
35. S. K. Das, S. Xu, A. Emwas, Y. Y. Lu, S. Srivastava, and L. A. Archer, *Energy Environ. Sci.*, **5**, 8927 (2012).
36. D. T. Sawyer, *Oxford University Press: New York* (1991).
37. C. J. Allen, J. Hwang, R. Kautz, S. Mukerjee, E. J. Plichta, M. A. Hendrickson, and K. M. Abraham, *J. Phys. Chem. C*, **116**, 20755 (2012).
38. Y. Ein-Eli and A. Kraytsberg, *Nano Energy*, **2**, 468 (2013).
39. Y. Katayama, H. Onodera, M. Yamagata, and T. Miura, *J. Electrochem. Soc.*, **151**, A59 (2004).
40. A. I. Bhatt, A. S. Best, J. Huang, and A. F. Hollenkamp, *J. Electrochem. Soc.*, **157**, A66 (2010).
41. L. Grande, E. Paillard, G. Kim, S. Monaco, and S. Passerini, *Int. J. Mol. Sci.*, **15**, 8122 (2014).
42. C. J. Allen, S. Mukerjee, E. J. Plichta, M. A. Hendrickson, and K. M. Abraham, *J. Phys. Chem. Lett.*, **2**, 2420 (2011).
43. X. J. Huang, E. I. Rogers, C. Hardacre, and R. G. Compton, *J. Phys. Chem. B*, **113**, 8953 (2009).
44. S. F. Lux, S. S. Jeong, G. T. Kim, S. Passerini, M. Winter, and A. Balducci, *ECS Trans.*, **25**, 21 (2010).
45. C. O'Laoire, S. Mukerjee, E. J. Plichta, M. A. Hendrickson, and K. M. Abraham, *J. Electrochem. Soc.*, **158**, A302 (2011).
46. J. Christensena, P. Albertusa, R. S. Sanchez-Carrerab, T. Lohmanna, B. Kozinskyb, R. Liedtkec, J. Ahmeda, and A. Kojic, *J. Electrochem. Soc.*, **159**, R1 (2012).